ACS OMEGA

http://pubs.acs.org/journal/acsodf

Article

Sixteen Percent Solar-to-Hydrogen Efficiency Using a Power-Matched Alkaline Electrolyzer and a High Concentrated Solar Cell: Effect of Operating Parameters

Shahid M. Bashir, Muhammad A. Nadeem, Maher Al-Oufi, Mohannad Al-Hakami, Tayirjan T. Isimjan, and Hicham Idriss*

Cite This: *ACS Omega* 2020, 5, 10510−10518

Read Online

ACCESS | Metrics & More | Article Recommendations | Supporting Information

ABSTRACT: The effect of electrode area, electrolyte concentration, temperature, and light intensity (up to 218 sun) on PV electrolysis of water is studied using a high concentrated triple-junction (3-J) photovoltaic cell (PV) connected directly to an alkaline membrane electrolyzer (EC). For a given current, the voltage requirement to run an electrolyzer increases with a decrease in electrode sizes (4.5, 2.0, 0.5, and 0.25 cm^2) due to high current densities. The high current density operation leads to high Ohmic losses, most probably due to the concentration gradient and bubble formation. The EC operating parameters including the electrolyte concentration and temperature reduce the voltage requirement by improving the thermodynamics, kinetics, and transport properties of the overall electrolysis process. For a direct PV−EC coupling, the maximum power point of PV (P_{max}) is matched using EC $I-V$ (current−voltage) curves measured for different electrode sizes. A shift in the EC $I-V$ curves toward open-circuit voltage (V_{oc}) reduces the P_{op} (operating power) to hydrogen efficiencies due to the increased voltage losses above the equilibrium water-splitting potential. The solar-to-hydrogen (STH) efficiencies remained comparable (∼16%) for all electrode sizes when the operating current (I_{op}) was similar to the short-circuit current (I_{sc}) irrespective of the operating voltage (V_{op}), electrolyzer temperature, and electrolyte concentration.

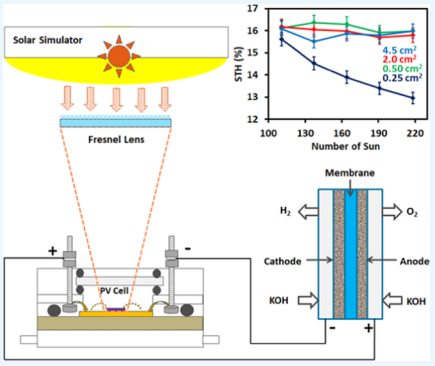

1. INTRODUCTION

Due to recent advancements in high concentrated solar cell technology, it is now possible to produce hydrogen in a bulk amount per unit of the photovoltaic cell (PV) area by integrating solar cells with an electrolysis process.[1−5] Unlike Si cells, multijunction solar cells (MJSCs) based on III−V group elements are capable of generating more power on a smaller area when operated at a higher concentration of sunlight.[6] Although the size of MJSC- and Si cell-based modules remains comparable due to the optical components used for receiving and focusing the light, an overall active area cell management is significantly reduced in the former case. Furthermore, higher efficiencies of MJSCs of up to ∼47% (now and with potential greater than 80% in the future) vs. a saturated maximum of ∼30% for the Si solar cells[7] encourage researchers to explore an integrated high concentrated PV−electrolysis system at laboratory and pilot plant scales[8] for the future. Both proton-exchange membranes (PEMs) and alkaline electrolyzers can be employed to generate molecular hydrogen and oxygen during PV−electrolysis. PEM electrolyzers offer high efficiencies but work only with expensive noble metals. Conventional alkaline electrolyzers, on the other hand, use nonprecious metals but suffer from low efficiencies and gas crossover issues.[9−11] Masel and co-workers have recently developed an anion-exchange membrane (Sustainion) that operates at high current densities (1 A/cm^2 at 2.2 V), outperforming the available commercial anion-exchange membranes.[12,13]

The efficiency of a PV−electrolysis process depends on the individual characteristics of the electrolyzer and the PV cell. In such a system, the power generated by the PV cell is converted into hydrogen, often expressed as power-to-hydrogen, by integrating the electrolyzer (EC) at the maximum power output (P_{max}) of the PV, either directly or through power electronics. MJSC provides much higher voltages than needed to overcome the minimum thermodynamic potential for the water-splitting reaction (1.48 V high heating value (HHV) or 1.23 V low heating value (LHV)). To utilize P_{max}, the PV $I-V$ curve should match the EC $I-V$ curve. A typical high concentrated triple-junction PV cell generates an open-circuit voltage of more than 3.0 V, which corresponds to a maximum usable voltage of ∼2.5−2.8 V, well above the operation range of an alkaline electrolyzer.

Received: February 20, 2020
Accepted: April 16, 2020
Published: April 28, 2020

https://dx.doi.org/10.1021/acsomega.0c00749
ACS Omega 2020, 5, 10510−10518

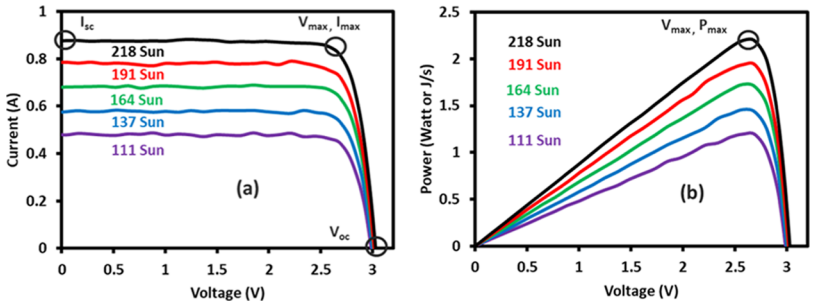

Figure 1. Effect of sun concentration on the characteristics of the Solar Junction Corporation triple-junction (3-J) solar cell at 60 °C: (a) Current−voltage (*IV*−PV) curves and (b) Power−voltage (P_wV−PV) curves. The area of the solar cell is 0.316 cm^2.

To match the EC *I*−*V* curve with P_{max}, three different strategies can be employed. First, output parameters from the PV cell can be tuned by installing a DC−DC convertor in between the EC and PV cell. This is done by interplaying with the voltage and current characteristics of PV at a similar power output. As a result, the excess (unused) voltage from the PV is stepped down with an enhancement in the total current at the same time.[14−20] Although this procedure is widely adopted by the PV−electrolysis community, the high cost and the additional resistance losses due to the power electronics adversely affect the economics of the overall process.[21] Second, the operating point of an electrolyzer can be matched using a dual-junction cell, which generates a maximum power at about ∼2.0 V, sufficient to run an alkaline electrolyzer. However, at the moment, the reported efficiency of dual-junction solar cells at high concentrations is low compared to that of multi-junction solar cells.[8,22,23] Finally, for a given PV, PV−EC power matching is also possible by tuning the characteristics of the electrolyzer. The temperature, gap between electrodes, electrolyte concentration, and size of the electrolyzer (or electrode assembly) are key parameters that alter the *I*−*V* curves of an EC. An optimal size of an EC for direct PV−EC coupling reduces the amount of the electrocatalyst used and thus the overall cost of the process.[2,4,24,25] An increase in temperature and electrolyte concentration enhances the performance of the electrolyzer by shifting the operating voltage to lower values at similar operating current densities. An increment in temperature reduces the thermodynamic potential for the water-splitting reaction due to the change in the Gibbs free energy (ΔG). For instance, an increase in temperature from 22 to 60 °C decreased the value of ΔG from ∼237 kJ/mol (1.23 eV) to ∼231 kJ/mol (1.19 eV). Likewise, the higher concentration of the electrolyte enhances the conductivity, which lowers the resistance due to the movement of ions. For example, the specific conductivity of KOH at 25 °C changes from 0.00243 S/cm at 0.01 M to 0.5603 S/cm at 5.0 M, with the effect of concentration being more prominent at higher temperatures.[26,27] The spatial separation between electrodes also adversely affects the electrolyzer performance.[10] Recent developments in anion-exchange membranes have opened up a new channel to operate an alkaline electrolyzer in a near-zero-gap configuration.

The high concentrated PV−electrolysis system has been widely explored in the past two decades, for which different power-matching techniques have been adopted. For instance, Chang and co-workers reported an electrical power-to-hydrogen efficiency of 78% and a solar-to-hydrogen efficiency (STH) of ∼21% at ∼1 sun using a single-junction GaAs solar cell and a DC−DC convertor in the PV−EC system.[15] Nakamura and co-workers reported an STH of 24.4% using concentrated photovoltaic and electrolysis systems coupled directly without any electronics. The maximum power matching was done by optimizing the ratio of the number of electrolyzers to PV cells.[2] The highest STH of ca. 30% has recently been reported on a laboratory scale by Jaramillo and co-workers through direct coupling of two PEM electrolyzers with one PV cell at 42 sun. While many attempts have been made to optimize the PV−EC system, the effects of operating parameters and light concentration have seldom been addressed in a systematic manner.

In this work, PV and electrolyzer cells are thoroughly characterized together and separately to extract the needed information. The understanding developed from the individual systems is applied to the PV−EC coupled system. Their data are presented and discussed with some details in this work.

2. RESULTS AND DISCUSSION

2.1. Characterization of a PV Cell. Figure 1 presents the effect of solar flux on the *I*−*V* characteristics of the PV cell measured at 60 °C. Although the PV cell was cooled through forced air convection along with a heat sink (Cu block), it was difficult to maintain the temperature of the PV cell below 60 °C for long periods. Therefore, the performance of the solar cell was evaluated at 60 °C to extract the PV characteristics, i.e., under real experimental conditions. The PV−EC coupling experiments were also carried out at the same PV temperature. In Figure 1a,b, a noticeable increase in I_{sc} (short-circuit current) and P_{max} (maximum possible output power) and a marginal increase in V_{oc} (open-circuit voltage) with increasing light concentration are observed.

The short-circuit current from a solar cell depends linearly on the solar concentration; thus, it does not affect the solar cell efficiency. The efficiency increase arises from the logarithmic dependence of the open-circuit voltage on the increase in incident light intensity.[28,29] This increase in voltage is given by

$$V_{OC,\,x} = \frac{nkT}{q}\ln\left(\frac{I_{sc}}{I_o}\right) + \frac{nkT}{q}\ln x \quad (1)$$

$$V_{OC,\,x} = V_{OC} + \frac{nkT}{q}\ln x \quad (2)$$

where $V_{oc,x}$, n, k, T, q, I_{sc}, I_o, x, and V_{oc} are open-circuit voltage (V) at a given sun concentration, ideality factor, Boltzmann constant ($m^2kg/(s^2K)$), absolute temperature (K), elementary charge on an electron (C), short-circuit current (A) at 1 sun, dark saturation current (A), number of sun, and open-circuit voltage (V) at 1 sun, respectively.

https://dx.doi.org/10.1021/acsomega.0c00749
ACS Omega 2020, 5, 10510−10518

Table 1. Effect of Solar Light Flux on PV Cell Characteristics Measured at 60 °C

				4			V_{oc} (V) calculated	
no. of sun (x)	V_{oc} (V) experimental	I_{sc} (A)	fill factor (FF)	I_o (A) calculated from eq 4	P_{max} (mW)	efficiency (%)	from eq 1	from eq 2
1	2.58	0.0039	85.1	1.15×10^{-22}	0.0085	27.1	2.58	2.58
111	2.98	0.48	84.9	1.44×10^{-23}	1.2	34.2	3.25	2.85
137	2.99	0.58	84.6	1.41×10^{-23}	1.46	33.9	3.27	2.87
164	3.01	0.68	84.9	1.30×10^{-23}	1.73	33.5	3.3	2.88
191	3.01	0.79	83.3	1.42×10^{-23}	1.95	32.4	3.31	2.88
218	3.02	0.88	82.6	1.22×10^{-23}	2.21	32.2	3.33	2.89

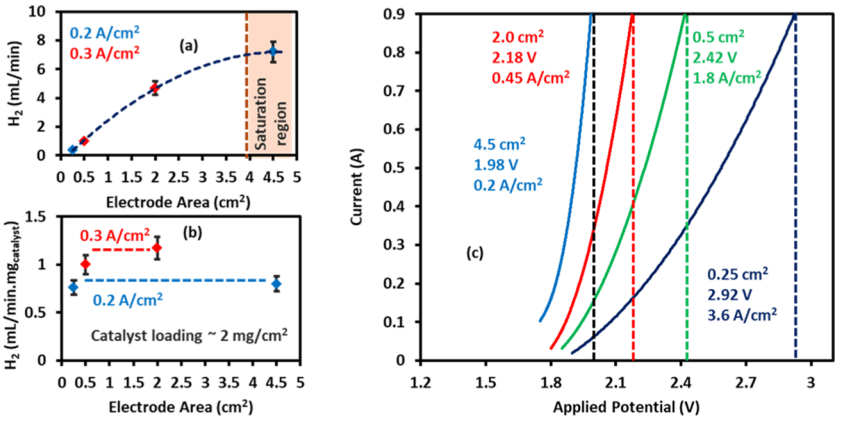

Figure 2. (a, b) Rate of H_2 (mL/min) and specific rate of H_2 (mL/(min.$mg_{catalyst}$)) production as a function of electrode sizes at the indicated current densities. (c) $I-V$ curves of the electrolyzer at 23 °C and under 1 M KOH concentration at different electrode areas. The area of the solar cell is 0.316 cm^2.

The efficiency of the PV cell increases from ∼27% at 1 sun to ∼34% at a concentration level of 111 sun; however, the change in efficiency with a further increase in the intensity is marginal at 60 °C as shown in Table 1. This is due to the usual change in the fill factor (FF) values. The FF of a solar cell at high flux may be reduced due to a few main reasons: (i) an increase in temperature that leads to a decrease in V_{oc}; (ii) increased losses in series resistance (R_s) due to an increase in the I_{sc}; (iii) a decrease in the shunt resistance (R_{sh}; the lowest-resistance pathway that allows current to flow through the PV cell circuit); and (iv) nonhomogeneous light distribution in the absence of a secondary optic (between the Fresnel lens and the cell) in this case. While V_{oc} is an intrinsic property of a semiconductor, R_s and R_{sh} are optimized during cell design. Probably all but (iv) would be constant, and we attribute the decrease in the FF to the increase in nonhomogeneous light with increasing intensity.

The $I-V$ curve of a solar cell is represented by a modified diode equation (eq 3). Light shifts the diode $I-V$ curve down into the fourth quadrant, where power can be extracted.

$$I = I_L - I_o \exp\left(\frac{qV}{nkT}\right) \quad (3)$$

where I, I_L, I_o, and V are the cell current, light-generated current, dark saturation current, and applied voltage, respectively. In eq 3, when there is no current flowing through the diode, $I = I_L = I_{sc}$. When all other parameters are known, I_o can be calculated using[29]

$$I_o = \frac{I_{sc}}{\exp^{(qV_{oc}/nkT)} - 1} \quad (4)$$

2.2. Characterization of the Alkaline Electrolyzer: Effect of Electrolyzer Size. Figure 2 shows the effect of the electrode area on the $I-V$ characteristics and hydrogen gas production during the electrolysis of water under basic conditions (pH 14.0). The aim is to understand the alkaline electrolyzer characteristics at different electrode area assemblies and use the knowledge gained to develop an optimized PV−electrolysis coupled system. In Figure 2a,b, the amount of hydrogen (mL/min) and the specific rate of hydrogen generation (mL/(min-$mg_{catalyst}$)) are presented as a function of electrode size (a catalyst loading of 2 mg/cm^2 on both electrodes). The catalyst loading of ∼2 mg/cm^2 is the reported value from the electrode manufacturer's publication, where the detailed procedure for the catalyst deposition is illustrated.[12,30] A loading of 2−5 mg/cm^2 is the typical value of non-noble metal-based electrocatalysts used in alkaline electrolyzers.[31]

The amount of hydrogen increases linearly with increasing electrode area up to 2 cm^2, at similar current densities (0.2 and 0.3 A/cm^2; well below the limiting current density regime), until it reaches its highest value at around 4.5 cm^2 (Figure 2a). The $I-V$ curves of electrolyzers at the indicated electrode sizes (0.25, 0.50, 2.0, and 4.5 cm^2) were generated using chronoamperometric measurements (Figure S4) by applying selected applied potentials for a given interval of time to get steady-state currents as well as quantifiable hydrogen and oxygen. The current density changed from 0.02 to 3 A/cm^2. To make a comparative analysis, the values of 0.2−0.3 A/cm^2 were opted because they were shared by all used catalysts. The small difference of 0.1 A/cm^2 between the values may not largely affect the analysis. The water-splitting reaction is a catalytic process in which the amount of product formed is proportional to the number of active sites. However, there is an optimal value beyond which the product formation does not

https://dx.doi.org/10.1021/acsomega.0c00749
ACS Omega 2020, 5, 10510−10518

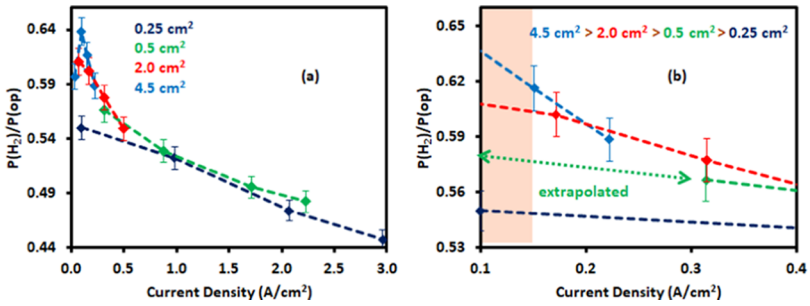

Figure 3. (a) Ratio of the power to hydrogen $P(H_2)$ as a function of current density at the indicated electrode size. (b) Inset of (a). The area of the solar cell is 0.316 cm^2.

change irrespective of the number of sites present. For instance, the number of sites on the oxygen evolution reaction (OER) side ($NiFe_2O_4$) is 1.3×10^{18} on a 0.25 cm^2 area vs. 2.3×10^{19} on a 4.5 cm^2 electrode surface (calculated from the catalyst loading and electrode size, Table S1). This implies that, at a constant current density, a minimum number of sites are needed for maximum activity; for example, 2.3×10^{19} sites per 4.5 cm^2 in this case. One way of increasing the number of active sites on a smaller electrode is to consider higher loading of the catalyst per unit area of the support. In Figure 2b, the rates of hydrogen production normalized with respect to the amount of active catalytic material are plotted against the sizes of the electrode. It is noticed that at similar current densities the H_2 rate per mg of catalyst remains constant. For example, at a current density of 0.2 A/cm^2, the normalized H_2 rates at 4.5 and 0.25 cm^2 differ only by 3%, which is within the experimental error limits. This suggests that the catalyst loading is optimal, under given experimental conditions, and the drop in activity at small electrode sizes is related to other factors. While the electrochemical active surface (ECSA) measurement is an appropriate way of determining active sites, because the study is carried out on the same electrocatalyst (loaded on the same substrate) having similar geometrical and morphological structure and tested under similar experimental conditions, we assumed that changing the geometric area does not affect any other property.

Figure 2c shows the $I-V$ curve of the alkaline electrolyzer as a function of electrode size. Increasing the electrode area shifted the $I-V$ curves to a lower voltage, at a fixed current value. For example, a current of 0.9 A is generated by a 0.25 cm^2 electrode at an applied potential of 2.92 V; the latter is reduced significantly to a value of 1.98 V at an electrolyzer size of 4.5 cm^2. However, the current density values increase from 0.2 A/cm^2 with a 4.5 cm^2 electrode to 3.6 A/cm^2 with a 0.25 cm^2 electrode. A typical alkaline electrolyzer safely operates between 1.0 and 1.5 A/cm^2. Since the rate of hydrogen production per unit area is proportional to the amount of current generated per unit area (i.e., current density), an increase in current density leads to a higher resistance at the electrode/electrolyte interface.

The effect of the electrolyzer efficiency on current density is further elaborated in Figure 3. When an electrolyzer is operated with a small electrode, the efficiency losses are more significant, especially at higher current densities; the effect is less pronounced in the case of larger electrodes due to low current densities. Similar electrocatalysts are used to study the effect of electrode size to account for the activation overpotential when normalized to active sites (Figure 2b). During operation, hydrogen and oxygen bubbles are continuously formed on their respective electrode surfaces. The presence of these bubbles prevents access of the ionic species to the active sites. The resistance due to bubbles is physically noticed in the form of a noisy background during chronoamperometric measurement with 0.25 cm^2, as shown in Figure S4. This induces mass transfer resistance, leading to the overpotential rise.

In addition to the voltage increase during operation with smaller electrode areas, a decay in the activity and ultimately short circuiting of the electrolyzer were noticed when experiments were carried out for a longer period of time. Physical damage to the electrodes including cracks and crevices was observed with the naked eye toward the end of the reaction. It is reported that hydrogen bubbles tend to grow at scratches, thereby creating additional stress on the electrode surface.[32] Pinholes and cracks are also formed in the polymeric membrane at high-current-density operations, which enhances the rate of gas crossover.

The voltage requirement of an electrolyzer increases with increasing current density. This increase has been modeled and is found to depend on different resistances in the electrolyzer and a kinetic parameter, K. The latter is defined below. The choice of the operating point should depend on the maximum overall conversion efficiency to yield the highest hydrogen output at a given solar irradiation and minimized investment cost for the highly concentrated PV−electrolysis system. If the equilibrium potential for an electrochemical power source is E_o and the operating potential at electrodes is V_{op}, then, according to the general rule of power generation from electrochemical power sources, the power (P) produced can be expressed by[33,34]

$$P \propto (E_o - V_{op})^2 \tag{5}$$

Equation 5 is used to calculate the power generated using fuel cells. For water electrolysis, this equation can be modified to

$$P \propto (V_{op} - E_o)^2 \tag{6}$$

In water electrolysis, a combination of different resistances influences its power efficiency. These include Ohmic resistance and concentration resistance. If the sum of the resistances of an electrolytic cell is R, the total potential drop for the whole cell is IR when current passes through it. The detailed derivation of these potential drops is given in the Supporting Information. Thus, the practical potential experienced by electrodes becomes equal to V_{op} reduced by the voltage drop over the cell resistance. In view of the above situation, eq 6 is modified and expressed as

https://dx.doi.org/10.1021/acsomega.0c00749
ACS Omega 2020, 5, 10510−10518

$$P = K(V_{op} - IR - E_o)^2 \quad (7)$$

K is the proportionality coefficient of power conversion and reflects the capability of an electrolyzer to convert electrical energy into chemical energy. Different electrolytic cells with various operating conditions, such as pressure, temperature, and catalyst loading, have different values of K. From a dimensional analysis, the unit of power conversion coefficient is 1/Ohm. Considering the power consumed by the cell resistance (I^2R), the power applied follows

$$IV_{op} - I^2R = K(V_{op} - IR - E_o)^2 \quad (8)$$

From eq 8, the relationship between I and V can be obtained using

$$I = \frac{V_{op} + 2KR(V_{op} - E_o) - \sqrt{V_{op}^2 + 4KRE_o(V_{op} - E_o)}}{2R(1 + KR)} \quad (9)$$

Equation 9 expresses the performance of an electrolytic cell. The parameters R and K influence the performance of an electrolyzer, as shown in Figure 4.

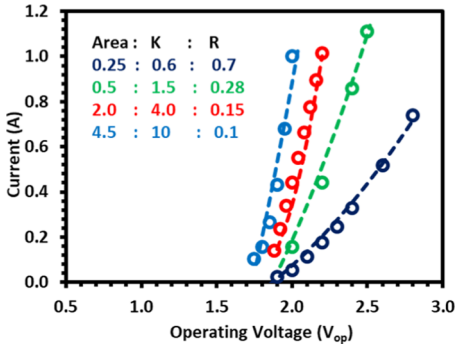

Figure 4. Effect of the membrane electrode assembly (MEA) and size on the electrolyzer $I-V$ curves. Solid lines were obtained using eq 9. The markers represent the experimental electrolyzer $I-V$ curves taken from Figure 2.

The value of resistance R is relevant to the slope of the electrolysis curve. The value of kinetic parameter K influences both the slope and the shape of the electrolysis curve within the $0 \leq K < \infty$ limit. Considering an extreme condition, when the value of $K = 0$, eq 9 changes to $I = 0$, indicating no kinetic activities of electrodes. When the value of $K = \infty$, eq 9 becomes

$$I = \frac{(V_{op} - E_o)}{R} \quad (10)$$

Equation 10 represents a line that passes through the point (E_o, 0) with a slope of $1/R$. It means that an electrochemical cell behaves like an Ohmic resistor if the overall kinetic activity (represented by K) of electrodes approaches infinity. Figure 4 indicates that there is an increase in the electrolyzer resistance and a corresponding decrease in the kinetic parameter with a decrease in its size. The shift in $I-V$ curves is due to the change in the parameters introduced by the size of the membrane. In this case, the resistance due to wires and current collectors can be neglected, as these components remained unchanged. As noted earlier from the specific rate of H_2 production from the similar surfaces, it appears that the kinetic parameter does not depend on the intrinsic catalytic activity of the system. This may indicate that the change in the $I-V$ curve is governed by the concentration resistance of the solution and the bubble effect that controls the flux of the OH^- ion on the electrode surface. At small electrode sizes, a higher active species flux is obtained; thus, a high voltage is needed to maintain a current similar to that obtained at larger electrode areas.

2.3. Direct PV–Electrolyzer Coupling. The typical $I-V$ characteristics of an alkaline electrolyzer and a III–V multijunction solar cell are shown in Figure 5, with the intersection of the two curves representing the operating point (P_{op}). The choice of P_{op} is important as it maximizes the overall conversion efficiency at a given solar irradiation and therefore minimizes the investment cost for the high concentrated PV–electrolysis system. The solar cell generates high output currents within a broad voltage range, and the current consumption of the electrolyzer increases exponentially with increasing voltage. There is a shift in P_{op} toward the higher voltage with a decrease in electrode area due to the reasons noted previously. STH does not change for electrode areas above 0.5 cm^2 where any difference noted is within the experimental error limit. A similar STH is due to P_{op} being below P_{max}, generally a point at which the difference in current generated from a solar cell as a function of applied voltage is negligible, at a given sun concentration. The small STH for the 0.25 cm^2 electrode area is due to P_{op} being below P_{max}, which results in I_{op} being significantly less than I_{sc}. The difference in I_{op} increases with increasing sun concentration. The STH of a PV–EC coupled system mostly depends on I_{op}, which is always situated at a voltage equal to the equilibrium water splitting voltage plus the electrolyzer overpotential.

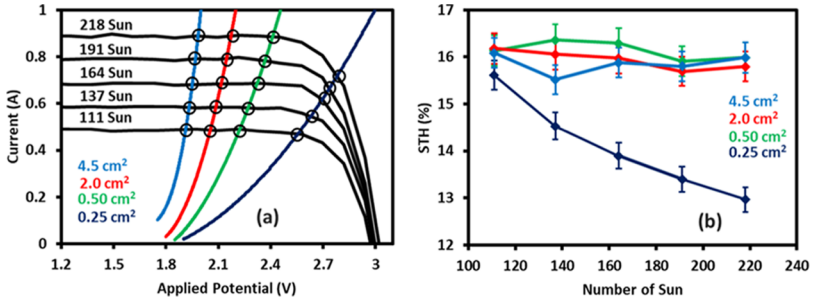

Figure 5. PV–EC coupling: (a) PV $I-V$ and EC $I-V$ curve coupling and (b) STH under different sun concentrations and electrode areas and at an electrolyzer temperature of 23 °C. The area of the solar cell is 0.316 cm^2.

https://dx.doi.org/10.1021/acsomega.0c00749
ACS Omega 2020, 5, 10510–10518

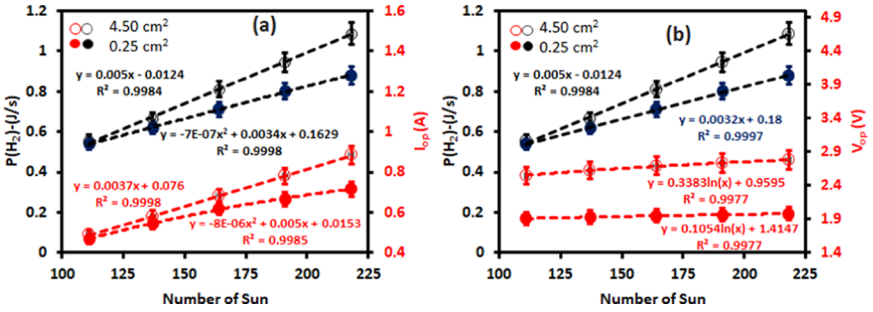

Figure 6. Effect of sun concentration on (a) I_{op} and the corresponding $P(H_2)$ and (b) V_{op} and the corresponding $P(H_2)$.

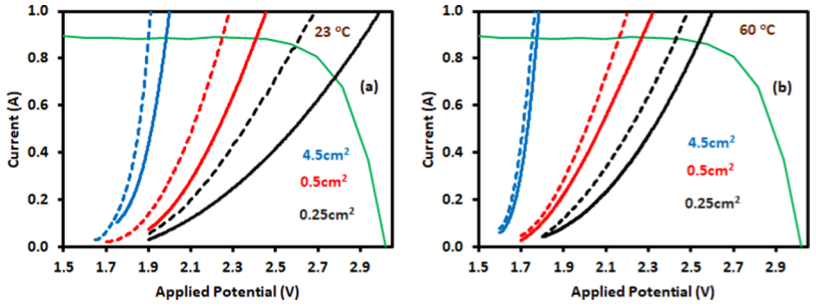

Figure 7. Effect of electrolyte concentration (1 M KOH solid line and 5 M KOH dashed line) on PV $I-V$ characteristics for different electrodes areas at electrolyzer temperatures of (a) 23 °C and (b) 60 °C.

Figure 6 Further elaborates the above-discussed points. $P(H_2)$ is calculated using11

$$P(H_2) = \Delta G \times nH_2 \quad (11)$$

where ΔG is the free energy change of the molecular hydrogen and oxygen reaction to liquid water (237 kJ/mol) and nH_2 is the molar flow of hydrogen produced. The STH in this case is the ratio of the P_{H_2} and the applied simulated solar power. Three points are worth noting in Figure 6a. (1) For the 4.5 cm^2 area, I_{op} has a linear dependency on sun concentration following the typical solar cell behavior. (2) In the case of the 0.25 cm^2 area, current shows nonlinear behavior due to nonoptimized PV−EC coupling. (3) In both cases, $P(H_2)$ follows the I_{op} trend, indicating that $P(H_2)$ depends on I_{op}. In Figure 6b, two further points are worth noting. (1) V_{op} shows logarithmic behavior for both electrode areas following typical solar cell behavior (although a quadratic fit is also possible); however, P_{H_2} is linear in the case of the 4.5 cm^2 area. (2) There is higher V_{op} and lower $P(H_2)$ in the case of the 0.25 cm^2 electrode area as compared to the 4.5 cm^2 area, in which case the relationship is opposite. This indicates that $P(H_2)$ is independent of V_{op}.

Figure 7 presents the electrolyte concentration and temperature effects of the EC on the PV $I-V$ characteristics with different electrode areas. Experiments were carried out at electrolyzer temperatures of 23 and 60 °C with 1 M and 5 M KOH, respectively. We have used 5 M KOH concentration for the purpose of comparison. Overall, an increase in the electrolyte concentration and reaction temperature leads to an improvement in the electrolyzer performance by reducing the voltage needed for the reaction. Higher electrolyte concentrations improve the charge transport properties (ion diffusion and migration) and ionic conductivity of the solution and thus influence the kinetics of the process.[10,35] In Figure 7a,b, when the electrolyte concentration changes from 1 to 5 M, an increase in the current response is noticed at different applied potentials on 0.25, 0.5, and 4.5 cm^2 electrode areas. Although a change in the concentration alters the operating voltages, the effect is gradually more visible on smaller electrode areas and at similar operating current values. For instance, at a current of 0.6 A, the voltage drop in the case of 0.5 cm^2 (1.2 A/cm^2) is ∼0.14 V compared to ∼0.08 V for the 4.5 cm^2 (0.13 A/cm^2) electrode area at 23 °C (Figure 7a).

High molar concentrations of KOH bring 3.8 and 3.0% increases in the power-to-hydrogen efficiencies, when measured at similar current densities of ∼0.2 A/cm^2 (4.5 cm^2) and ∼0.3 A/cm^2 (0.5 cm^2), respectively. The small difference in the efficiency increase is due to the low operational current densities. It was not possible to run the electrolyzer at higher current densities with the 4.5 cm^2 area electrolyzer due to the current limitation of our electrochemical workstation. However, it is likely that at higher current densities an increase in electrolyte concentration would further enhance the efficiencies, as observed in the $I-V$ characteristics of the alkaline electrolyzer (Figure 7) under such conditions. In a further attempt to study the effect of temperature at a given electrolyte concentration, we have computed part of the data presented in Figure 7, as shown in Table 2. In line with other studies,[38,39] while the entropy of activation contribution is small, the $T\Delta^{\ddagger}S$ is a large component of the free energy of activation, $\Delta G^{\ddagger}$.

3. CONCLUSIONS

For direct PV−electrolysis, an optimized coupling of the two systems is needed to achieve the highest possible STH. Once a PV cell has an operating voltage (V_{op}) equal to the sum of equilibrium water-splitting potential (V_{eq}) and overall electrolyzer overpotential (η), the STH is determined solely by the operating current (I_{op}). Maximum I_{op} can be obtained by designing a PV cell with maximum power (P_{max}) at V_{op} of an alkaline electrolyzer. Another strategy to obtain a high STH is to use multiple electrolyzers in series. In this case, the PV

https://dx.doi.org/10.1021/acsomega.0c00749
ACS Omega 2020, 5, 10510−10518

Table 2. Change in Entropy, $\Delta^{\ddagger}S$, and Free Energy, $\Delta^{\ddagger}G$, of Activation with Temperature at 1 M KOH for the Overall Reaction Using FeNiCo Alloy Nanoparticles as the Cathode, Spray-Coated on a Porous Carbon and a Stainless Steel Fiber Belt Coated with $NiFe_2O_4$ as the Anode[d]

temperature (K)	$\Delta^{\ddagger}H$ (kJ/mol)[a]	j (A/m^2)	$\Delta^{\ddagger}S$ (J/mol·K)[b]	$T\Delta^{\ddagger}S$ (kJ/mol)	$\Delta^{\ddagger}G$ (kJ/mol)[c]
293	17.2	1391	−284.0	−83.2	100.4
343	17.2	3958	−285.2	−97.8	115

[a] $\Delta^{\ddagger}H = \Delta^{\ddagger}H^{o} - \alpha F\eta$; η = 0.7 V; α = 0.45 (calculated from the slope of $\Delta^{\ddagger}H$ vs η); $\Delta^{\ddagger}H$ is computed from the slope (×2.3R) of log(j) as a function of 1/T, $\Delta^{\ddagger}H^{o}$ is calculated from the intercept of $\Delta^{\ddagger}H$ vs η, α is the charge transfer coefficient, and η is the overvoltage. [b] $\Delta^{\ddagger}S$ is calculated from the equation $\Delta^{\ddagger}S = 2.3R[\log(j) + \Delta^{\ddagger}H/2.3RT - \log(nF\omega C_{KOH})]$, where $\omega = kT/h$, ω is the frequency term, and n = 2. [c] $\Delta^{\ddagger}G = \Delta^{\ddagger}H - T\Delta^{\ddagger}S$. [d][KOH] = 1 M; C, concentration; j, current density (A/m^2); F, Faraday's constant (96 485 C/mol of electrons); k_B, Boltzmann's constant (1.38 10^{-23} J/K); h, Planck's constant (6.62 10^{-34} J s); T, temperature in K; and R, gas constant (8.314 J/mol K).

voltage at maximum power (V_{max}) should match the sum of the V_{op} for all electrolyzers. V_{op} of an electrolyzer can be changed using different electrode sizes, electrolyte concentrations, and temperatures. However, each of these parameters has its limit. At an optimized electrode area where V_{op} is close to V_{eq} and electrolyzer η, the maximum temperature is limited by the stability of membrane. At about 60 °C, the electrolyte concentration effect above 1 M is found to be negligible once the electrocatalyst is in excess (the 4.5 cm^2 case). Each given electrocatalyst can be characterized to have an upper and a lower current density limit. Above the upper limit, the catalyst starts to drive high overpotential with simultaneous degradation. On the other hand, any decrease in the current density below the lower limit has a negligible effect on V_{op}, indicating that a decrease in current density by increasing the electrode area below this limit has a negligible effect on PV−EC power matching.

4. EXPERIMENTAL SECTION

Figure S1 shows a diagram of the solar cell assembly (SCA) used in this work. Briefly, the SCA comprises the following components: (1) a solar simulator as a light source; (2) a Fresnel lens as a concentrating optics; (3) a three-dimensional (3-D) printed plastic casing to cover a solar cell; (4) a quartz window to allow transmission of the complete spectrum of light; (5) copper clips to make external contact with the anode and cathode of the cell; (6) a triple-junction (3-J) solar cell (GaInP/GaAs/GaInAsNSb on a GaAs substrate) from Solar Junction (SJ) Corporation; (7) a copper block as a heat sink; (8) low-resistance copper cables to minimize losses; (9) a thermocouple installed in close proximity to the cell to measure its temperature; and (10) air flow channels for further cooling the cell. The purpose of encapsulating the solar cell is to protect it from deterioration since it is susceptible to surface reaction/degradation under light illumination if exposed to atmospheric humidity for long periods.[36,37] Therefore, solar cell enclosure was initially evacuated before final sealing. The solar concentration was determined using the geometric area of the Fresnel lens and the concentrated spot at the solar cell position as described in the Supporting Information section (Figure S2).

Figure S3 shows an experimental setup used to characterize an alkaline electrolyzer for water splitting. A 5 cm^2 metallic chassis electrolyzer body was obtained from Dioxide Materials, Florida. Both electrodes (i.e., cathode and anode substrates coated with electrocatalysts) were purchased from the same manufacturer and used without further modifications. The cathode layer was composed of FeNiCo alloy nanoparticles, which were spray-coated on a carbon-based gas diffusion layer, while a stainless steel fiber belt coated with $NiFe_2O_4$ particles was used as the anode.[12] An alkaline membrane (Sustainion from Dioxide materials) activated overnight by soaking in (1 M) KOH solution was sandwiched between these two catalyst layers to form a membrane electrode assembly (MEA). During operation, the KOH (1 M) solution was circulated in catholyte and anolyte compartments using a peristaltic pump at a flow rate of 3 mL/min. An Autolab potentiostat and Extech power supply were used to supply electrical power to the electrolyzer, when used alone, while the Hofmann displacement method was used to measure the volumetric amount of hydrogen and oxygen gases. To ensure the accuracy in the measurement, a few gas samples were also analyzed using gas chromatography (GC). To monitor H_2, a gas chromatograph (Agilent Technologies, 7890A) equipped with a thermal conductivity detector (TCD) connected to a Porapak Q packed column (2 m long, 1/8 in. external diameter) at 45 °C was used with N_2 as the carrier gas (flow rate, 20 mL/min; pressure, 8 psi). Oxygen was monitored using another GC (Thermo Scientific, Trace1300) equipped with a TCD connected to a packed molecular sieve (5A) column (2 m long, 1/8 in. external diameter) with He as the carrier gas (flow rate, 1.5 mL/min; pressure, 22 psi).

The efficiency of an alkaline water electrolyzer was measured using the amount of hydrogen generated and the operating power (operating voltage x operating current). Different electrode sizes of 0.25, 0.5, 2.0, and 4.5 cm^2 were used to study the size effect. In the case of electrodes smaller than the size of the flow field or channels (4.5 cm^2), silicone rubber gaskets with appropriate sizes were installed inside the EC body to ensure that only the active electrode areas were in contact with the current collectors (reactor body and the electrolyte). The reaction was studied at different temperatures; the data reported here were collected at 23 and 60 °C. The overpotential of the anode was calculated separately and was found to be 0.25 ± 0.03 V at 10 mA/cm^2 under 1 M KOH at 23 °C. The overall overpotential (overvoltage) at the same condition is 0.47 ± 0.03 V, from which the cathodic overpotential was extracted, ca. 0.2 V.

The PV−electrolysis experiments were carried out by direct coupling of the PV cell with an electrolyzer, without a DC−DC convertor. The power matching of PV and an electrolyzer was done by measuring the I−V curves of the PV and the electrolyzer, separately. While the maximum power point of PV was fixed at each individual sun concentration, the operating power of the electrolyzer was brought closer to the P_{max} by changing the size of the electrodes, as indicated above.

■ ASSOCIATED CONTENT

Supporting Information

The Supporting Information is available free of charge at https://pubs.acs.org/doi/10.1021/acsomega.0c00749.

Diagram and schematic of a solar cell assembly (SCA), picture of the alkaline electrolyzer setup, chronoampero-

https://dx.doi.org/10.1021/acsomega.0c00749
ACS Omega 2020, 5, 10510−10518

metric measurements with different electrode sizes with 1 M KOH at 23 °C, and electrolyzer overpotential derivation (PDF)

AUTHOR INFORMATION

Corresponding Author

Hicham Idriss − *Hydrogen Platform, SABIC Corporate Research and Development Center, KAUST, Thuwal 23955, Saudi Arabia;* orcid.org/0000-0001-8614-7019; Email: idrissh@sabic.com

Authors

Shahid M. Bashir − *Hydrogen Platform, SABIC Corporate Research and Development Center, KAUST, Thuwal 23955, Saudi Arabia;* orcid.org/0000-0002-3710-3068

Muhammad A. Nadeem − *Hydrogen Platform, SABIC Corporate Research and Development Center, KAUST, Thuwal 23955, Saudi Arabia*

Maher Al-Oufi − *Hydrogen Platform, SABIC Corporate Research and Development Center, KAUST, Thuwal 23955, Saudi Arabia*

Mohannad Al-Hakami − *Hydrogen Platform, SABIC Corporate Research and Development Center, KAUST, Thuwal 23955, Saudi Arabia*

Tayirjan T. Isimjan − *Hydrogen Platform, SABIC Corporate Research and Development Center, KAUST, Thuwal 23955, Saudi Arabia*

Complete contact information is available at: https://pubs.acs.org/10.1021/acsomega.0c00749

Notes

The authors declare no competing financial interest.

ACKNOWLEDGMENTS

The authors thank Solar Junction Corporation for providing a triple-junction solar cell free of cost.

REFERENCES

(1) Khaselev, O.; Bansal, A.; Turner, J. A. High-efficiency integrated multijunction photovoltaic/electrolysis systems for hydrogen production. *Int. J. Hydrogen Energy* **2001**, *26*, 127−132.

(2) Nakamura, A.; Ota, Y.; Koike, K.; Hidaka, Y.; Nishioka, K.; Sugiyama, M.; Fujii, K. A 24.4% solar to hydrogen energy conversion efficiency by combining concentrator photovoltaic modules and electrochemical cells. *Appl. Phys. Express* **2015**, *8*, 107101−107104.

(3) Fujii, K.; Nakamura, S.; Sugiyama, M.; Watanabe, K.; Bagheri, B.; Nakano, Y. Characteristics of hydrogen generation from water splitting by polymer electrolyte electrochemical cell directly connected with concentrated photovoltaic cell. *Int. J. Hydrogen Energy* **2013**, *38*, 14424−14432.

(4) Jia, J.; Seitz, L. C.; Benck, J. D.; Huo, Y.; Chen, Y.; Ng, J. W. D.; Bilir, T.; Harris, J. S.; Jaramillo, T. F. Solar water splitting by photovoltaic-electrolysis with a solar-to-hydrogen efficiency over 30%. *Nat. Commun.* **2016**, *7*, No. 13237.

(5) McConnell, R.; Thompson, J. In *Generating Hydrogen Through Water Electrolysis Using Concentratorphotovoltaic*, DOE Solar Energy Technologies, Program Review Meeting Denver, Colorado, 2004.

(6) Cotal, H.; Fetzer, C.; Boisvert, J.; Kinsey, G.; King, R.; Hebert, P.; Yoon, H.; Karam, N. III−V multijunction solar cells for concentrating photovoltaics. *Energy Environ. Sci.* **2009**, *2*, 174−192.

(7) Andreani, L. C.; Bozzola, A.; Kowalczewski, P.; Liscidini, M.; Redorici, L. Silicon solar cells: toward the efficiency limits. *Adv. Phys.: X* **2019**, *4*, No. 1548305.

(8) Green, M. A.; Hishikawa, Y.; Dunlop, E. D.; Levi, D. H.; Hohl-Ebinger, J.; Yoshita, M.; Ho-Baillie, A. W. Y. Solar cell efficiency tables (Version 53). *Prog. Photovoltaics Res. Appl.* **2019**, *27*, 3−12.

(9) Ogawa, T.; Takeuchi, M.; Kajikawa, Y. Analysis of trends and emerging technologies in water electrolysis research based on a computational method: A comparison with fuel cell research. *Sustainability* **2018**, *10*, 478−501.

(10) Schalenbach, M.; Zeradjanin, A.; Kasian, O. I.; Cherevko, S.; Mayrhofer, K. A perspective on low-temperature water electrolysis-Challenges in alkaline and acidic technology. *Int. J. Electrochem. Sci.* **2018**, *13*, 1173−1226.

(11) Schalenbach, M.; Tjarks, G.; Carmo, M.; Lueke, W.; Mueller, M.; Stolten, D. Acidic or alkaline? Towards a New Perspective on the efficiency of water electrolysis. *J. Electrochem. Soc.* **2016**, *163*, F3197−F3208.

(12) Liu, Z.; Sajjad, S. D.; Gao, Y.; Yang, H.; Kaczur, J. J.; Masel, R. I. The effect of membrane on an alkaline water electrolyzer. *Int. J. Hydrogen Energy* **2017**, *42*, 29661−29665.

(13) Masel, R. I.; Liu, Z.; Yang, H.; Sajjad, S. D.; Gao, Y.; Kaczur, J. J. A high performing zero gapalkaline electrolyzer. ECS Meeting Abstracts MA2017-02 1006-1006 2017.

(14) Dahbi, S.; Aboutni, R.; Aziz, A.; Benazzi, N.; Elhafyani, M.; Kassmi, K. Optimised hydrogen production by a photovoltaic-electrolysis system DC/DC converter and water flow controller. *Int. J. Hydrogen Energy* **2016**, *41*, 20858−20866.

(15) Chang, W. J.; Lee, K.-H.; Ha, H.; Jin, K.; Kim, G.; Hwang, S.-T.; Lee, H.-M.; Ahn, S.-W.; Yoon, W.; Seo, H.; Hong, J. S.; Go, Y. K.; Ha, J.-I.; Nam, K. T. Design principle and loss engineering for photovoltaic-electrolysis cell system. *ACS Omega* **2017**, *2*, 1009−1018.

(16) García-Valverde, R.; Miguel, C.; Martínez-Béjar, R.; Urbina, A. Optimized photovoltaic generator−water electrolyser coupling through a controlled DC−DC converter. *Int. J. Hydrogen Energy* **2008**, *33*, 5352−5362.

(17) Ota, Y.; Yamashita, D.; Nakao, H.; Yonezawa, Y.; Nakashima, Y.; Ebe, H.; Inagaki, M.; Mikami, R.; Abiko, Y.; Iwasaki, T.; Sugiyama, M.; Nishioka, K. Highly efficient 470 W solar-to-hydrogen conversion system based on concentrator photovoltaic modules with dynamic control of operating point. *Appl. Phys. Express* **2018**, *11*, 077101−077104.

(18) Sugiyama, M.; Nakamura, A.; Watanabe, K.; Ota, Y.; Nishioka, K.; Nakano, Y.; Fujii, K. In *Concentrated Photovoltaic Electrochemical Cell (CPEC): A Route Toward High-Efficiency, Cost-Effective Solar Hydrogen Production*, IEEE 42nd Photovoltaic Specialist Conference (PVSC), New Orleans, LA, 2015; pp 1−4.

(19) Wai, S. H.; Ota, Y.; Yamashita, D.; Sugiyama, M.; Nishioka, K. High efficiency solar to gas conversion system using concentrator photovoltaic and electrochemical cell. *Grand Renewable Energy Proc.* **2018**, *1*, No. 44.

(20) Yonezawa, Y.; Atsushi, M.; Nakao, H.; Takauchi, H.; Nakashima, Y.; Ebe, H.; Yamashita, D.; Sugiyama, M.; Ota, Y.; Nishioka, K. In *Model-Based Development of Solar-to-Hydrogen Conversion System with Dynamic Operating Point Control of Multiple DC-DC Converters*, 2018 7th International Conference on Renewable Energy Research and Applications (ICRERA), 2018; pp 1435−1440.

(21) Al-Sayegh, S.; Al-Salik, Y.; Katsiev, B.; Varijan, R.; Isimjan, T. T.; Idriss, H. Methanol production usingusing ultra high concentrated solar cells: Hybrid electrolysis and captured CO_2. *ACS Energy Lett.* **2020**, *5*, 540−544.

(22) Green, M. A.; Emery, K.; Hishikawa, Y.; Warta, W.; Dunlop, E. D. Solar cell efficiency tables (version 47). *Prog. Photovoltaics Res. Appl.* **2016**, *24*, 3−11.

(23) Frank, D.; Peharz, G.; Wittstadt, U.; Hacker, B.; Bett, A. In *Hydrogen Production in a PV Concentrator Using III-V Multi-Junction Solar Cells*, IEEE 4th World Conference on Photovoltaic Energy Conference, Waikoloa, HI, 2006.

(24) García-Valverde, R.; Espinosa, N.; Urbina, A. Optimized method for photovoltaic-water electrolyser direct coupling. *Int. J. Hydrogen Energy* **2011**, *36*, 10574−10586.

(25) Ohlmann, J.; Sanchez, J. F. M.; Lackner, D.; Förster, P.; Steiner, M.; Fallisch, A.; Dimroth, F. Recent development in direct generation of hydrogen using multi-junction solar cells. *AIP Conf. Proc.* **2016**, *1766*, No. 080004.
(26) Gilliam, R. J.; Graydon, J. W.; Kirk, D. W.; Thorpe, S. J. A review of specific conductivities of potassium hydroxide solutions for various concentrations and temperatures. *Int. J. Hydrogen Energy* **2007**, *32*, 359−364.
(27) Amores, E.; Rodríguez, J.; Carreras, C. Influence of operation parameters in the modeling of alkaline water electrolyzers for hydrogen production. *Int. J. Hydrogen Energy* **2014**, *39*, 13063−13078.
(28) Fedkin, M.; Dutton, J. A. Utility Solar Power and Concentration: 5.2. Light concentration effecton PV performance and efficiency, e-Education Institute, College of Earth and Mineral Sciences, Penn State University. https://www.e-education.psu.edu/eme812/node/538.
(29) Burhan, M.; Chua, K. J. E.; Ng, K. C. Long term hydrogen production potential of concentrated photovoltaic (CPV) system in tropical weather of Singapore. *Int. J. Hydrogen Energy Energy* **2016**, *41*, 16729−16742.
(30) Liu, Z.; Sajjad, S.; Gao, Y.; Kaczur, J.; Masel, R. I. An alkaline water electrolyzer with Sustainion membranes: 1 A/cm^2 at 1.9 V with base metal catalysts. *ECS Trans.* **2017**, *77*, 71−73.
(31) Wu, X.; Scott, K. A Li-doped Co_3O_4 oxygen evolution catalyst for non-precious metal alkaline anion exchange membrane water electrolysers. *Int. J. Hydrogen Energy* **2013**, *38*, 3123−3129.
(32) Westerheide, D. E.; Westwater, J. W. Isothermal growth of hydrogen bubbles during electrolysis. *AIChE J.* **1961**, *7*, 357−362.
(33) Shen, M.; Meuleman, W.; Scott, K. The characteristics of power generation of static state fuel cells. *J. Power Sources* **2003**, *115*, 203−209.
(34) Shen, M.; Bennett, N.; Ding, Y.; Scott, K. A concise model for evaluating water electrolysis. *Int. J. Hydrogen Energy* **2011**, *36*, 14335−14341.
(35) Xiang, C.; Papadantonakis, K. M.; Lewis, N. S. Principles and implementations of electrolysis systems for water splitting. *Mater. Horiz.* **2016**, *3*, 169−173.
(36) Hamdi, R. T. A.; Abdulhadi, S.; Kazem, H. A.; Chaichan, M. Humidity impact on photovoltaic cells performance: A review. *Int. J. Recent Eng. Res. Dev.* **2018**, *3*, 27−37.
(37) Mekhilef, S.; Saidur, R.; Kamalisarvestani, M. Effect of dust, humidity and air velocity on efficiency of photovoltaic cells. *Renewable Sustainable Energy Rev.* **2012**, *16*, 2920−2925.
(38) Lee, K.-G.; Balamurugan, M.; Park, S.; Ha, H.; Jin, K.; Seo, H.; Ki Tae Nam, K. T. Importance of Entropic Contribution to Electrochemical Water Oxidation Catalysis. *ACS Energy Lett.* **2019**, *4*, 1918−1929.
(39) Singh, R. N.; Lal, B. High surface area lanthanum cobaltate and its A and B sites substituted derivatives for electrocatalysis of O_2 evolution in alkaline solution. *Int. J. Hydrogen Energy* **2002**, *27*, 45−55.

https://dx.doi.org/10.1021/acsomega.0c00749
ACS Omega 2020, 5, 10510−10518